Bone 212 (2026) 118035

Contents lists available at ScienceDirect

Bone

journal homepage: www.elsevier.com/locate/bone

Full Length Article

Bone quality deteriorates in mice with pulmonary emphysema despite preserved open-field-assessed spontaneous locomotor activity

Takayuki Nabeshima [a], Manabu Tsukamoto [a,*], Ke-Yong Wang [b], Yosuke Mano [a], Daisuke Arakawa [a], Hitoshi Suzuki [a], Eiichiro Nakamura [a], Kazuhiro Yatera [c], Ryosuke Ozasa [d], Takayoshi Nakano [d], Akinori Sakai [a]

[a] Department of Orthopaedic Surgery, School of Medicine, University of Occupational and Environmental Health, 1-1 Iseigaoka, Yahatanishi-ku, Kitakyushu, 807-8555, Japan
[b] Shared-Use Research Center, School of Medicine, University of Occupational and Environmental Health, 1-1 Iseigaoka, Yahatanishi-ku, Kitakyushu, 807-8555, Japan
[c] Department of Respiratory Medicine, School of Medicine, University of Occupational and Environmental Health, 1-1 Iseigaoka, Yahatanishi-ku, Kitakyushu, 807-8555, Japan
[d] Division of Materials and Manufacturing Science, Graduate School of Engineering, The University of Osaka, 2-1 Yamadaoka, Suita, Osaka, 565-0871, Japan

ARTICLE INFO

Keywords:
Chronic obstructive pulmonary disease
Bone quality
Bone microstructure
Oxidative stress
Mouse model

ABSTRACT

Chronic obstructive pulmonary disease (COPD) is associated with an increased risk of fracture; however, the mechanisms underlying skeletal fragility in COPD remain incompletely understood. In particular, it is unclear whether bone deterioration is primarily attributable to physical inactivity or to intrinsic disease-related factors. In this study, we investigated the effects of emphysema on bone quality under conditions of comparable open-field-assessed spontaneous locomotor activity in an elastase-induced emphysema mouse model. Open-field-assessed spontaneous locomotor activity, feed intake, water intake, urine volume, and fecal volume did not differ between emphysema and control mice. In contrast, mice with emphysema exhibited impaired bone formation, deterioration of trabecular bone microstructure, and reduced bone material properties, including altered apatite *c*-axis orientation, the accumulation of advanced glycation end products, and increased bone brittleness. Exploratory cap analysis of gene expression sequencing of pooled bone marrow samples provided hypothesis-generating signals implicating mitochondrial and oxidative stress-related pathways. These results suggest that emphysema is associated with skeletal deterioration despite comparable open-field–assessed spontaneous locomotor activity and provide new insight into the mechanisms underlying fracture risk beyond bone mineral density in patients with chronic lung disease.

1. Introduction

Chronic obstructive pulmonary disease (COPD) is a lung disease that causes airflow obstruction and chronic respiratory symptoms triggered by long-term inhalation exposure to harmful substances, mainly smoking, resulting in organ damage throughout the body in addition to damage to the lungs [1,2]. COPD causes bone and muscle disorders such as extrapulmonary lesions [3–5] and is a risk factor for osteoporosis and fracture. The emphysema volume is negatively correlated with the bone mineral density (BMD) of the thoracic spine [6], and the severity of COPD is correlated with the BMD in each region [7]. In addition, epidemiological studies on COPD and fracture risk have reported a BMD-independent increase in fracture risk, and deterioration of bone quality has been suggested in patients with COPD [8].

Risk factors for musculoskeletal disorders in patients with COPD include aging, smoking, low body weight, physical inactivity, nutritional deficits, vitamin D deficiency, hypogonadism, decreased respiratory function, systemic inflammation, oxidative stress, hypoxia and glucocorticoid use [9]. As described in the “Clinical Practice Guide on Fracture Risk in Lifestyle Diseases”, the detailed pathological/molecular mechanisms of musculoskeletal complications in patients with COPD are unknown, and basic research is needed to elucidate these mechanisms [10]; however, verification in animal models and human bone biopsies has been limited, and the essential pathogenesis has not been elucidated.

We reported bone loss with decreased bone formation, muscle fiber atrophy and a shift in type from type I to type II muscle fibers in mice

* Corresponding author at: 1-1 Iseigaoka, Yahatanishi-ku, Kitakyushu, 807-8555, Japan.
E-mail address: m-tsuka@med.uoeh-u.ac.jp (M. Tsukamoto).

https://doi.org/10.1016/j.bone.2026.118035
Received 5 May 2026; Received in revised form 25 July 2026; Accepted 27 July 2026
Available online 29 July 2026

with emphysema induced by intratracheal elastase administration and reported that these findings were similar to the clinical picture in middle-aged and elderly patients with COPD [11,12]. We considered it appropriate to use a model to exclude general factors influencing bone metabolism and to investigate the effects of COPD/emphysema on bone; however, the spontaneous activity levels in this model were not evaluated. In addition, the material properties, which are the foundation of bone quality, have not been investigated.

In elastase-induced mice with emphysema, which are a model of relatively mild emphysema, we believe that spontaneous activity is not reduced. We hypothesized that mice with emphysema would demonstrate deterioration of bone quality (bone microstructure, bone metabolic dynamics, and material properties) even in the absence of detectable differences in open-field–assessed spontaneous locomotor activity. The purpose of our study was to investigate whether emphysema impairs bone quality under conditions of comparable open-field–assessed spontaneous locomotor activity.

2. Materials and methods

2.1. Animals

The experimental protocol was approved by the Ethics Review Committee for Animal Experimentation of our institution (approval number AE18–004). Mouse selection, anesthesia, and intratracheal administration procedures were performed as previously described [11]. A total of 30 eight-week-old male C57BL/6 J mice (approximately 20 g) were purchased from Charles River Japan (Tokyo, Japan) and acclimated for 4 weeks under standard laboratory conditions (temperature 24 ± 1 °C, humidity 55 ± 5%). All the mice were housed in similarly designed cages. The light/dark cycle was 12 h, with lights on from 7:00 a.m. to 7:00 p.m. Drinking water and feed were available ad libitum. All the mice were fed a commercial mouse diet (CE-2; Japan CLEA, Tokyo, Japan) containing 1.25% calcium and 1.06% phosphorus [13].

2.2. Experimental protocol

The experimental protocol design is shown in Fig. 1A. Mice aged 12 weeks (24–27 g) were anesthetized by an intraperitoneal injection of 0.3 mg/kg medetomidine (Kyoritsu Seiyaku Corporation, Tokyo, Japan), 1.0 mg/kg midazolam (Astellas Pharma Inc., Tokyo, Japan), and 5.0 mg/kg butorphanol (Meiji Seika Pharma Co., Ltd., Tokyo, Japan), followed by the intratracheal administration of 0.1 U of porcine pancreatic elastase (PPE; Sigma–Aldrich Inc., St. Louis, MO) dissolved in 50 μl of saline (PPE group) or 50 μl of saline alone (Saline group). The administration of PPE to both lungs of all the mice was confirmed by micro-CT (μCT). The mice were randomly allocated to the PPE or Saline groups. Blinding was not performed for group allocation or outcome assessment. To minimize potential assessment bias, outcomes were obtained using standardized protocols and predefined analysis procedures. Where applicable, image-based measurements were performed using fixed acquisition settings and predefined thresholds/parameters, and mechanical testing followed a prespecified protocol.

The body weights of the mice in each group were measured every week, and the amounts of drinking water, feed intake, urine, and feces were measured every 4 weeks for 24 h (from 9:00 a.m. to 9:00 a.m. the next day). In addition, pentosidine concentrations in urine (Japanese Institute for the Control of Aging, Fukuroi, Japan) were measured using urine collected at week 24. Spontaneous locomotor activity was

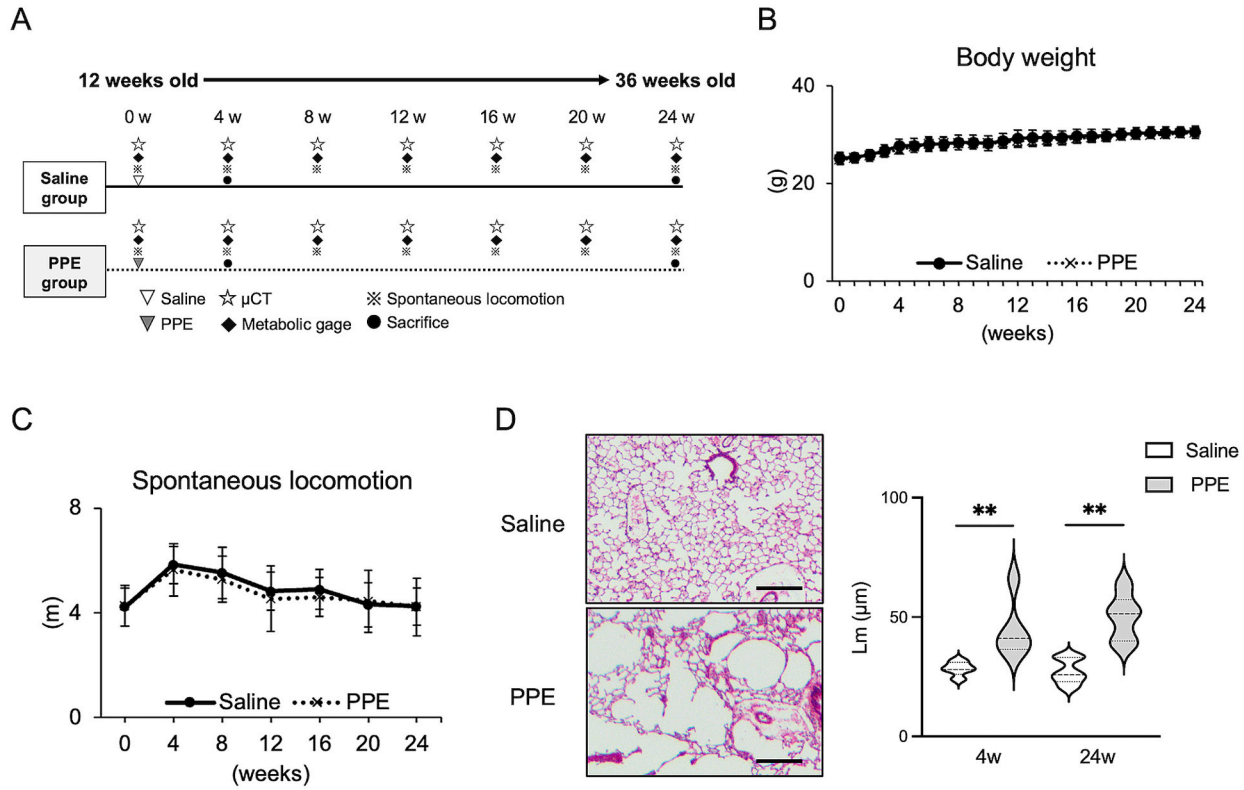

Fig. 1. Experimental protocol, body weight, open-field-assessed spontaneous locomotor activity, and lung morphometric analysis
(A) Experimental protocol. (B) Sequential changes in body weight. The data are presented as the mean ± SD ($n = 15$ mice per group). (C) Spontaneous locomotor activity measured every 4 weeks using an open-field test (400 × 400 × 400 mm) for 30 min with a video-tracking system (n = 15 mice per group). (D) Representative hematoxylin and eosin-stained lung sections. The mean linear intercepts (Lm) indicate the degree of pulmonary emphysema. Scale bar = 100 μm. Violin plots indicate the probability density of the kernel, and the width of the shaded areas represents the proportion of data. The thick dashed line in the center indicates the median, the box represents the interquartile range, and whiskers indicate min–max values. $^{**}P < 0.01$.

evaluated using the same procedure as in previous reports [14] and assessed every 4 weeks in an open field (400 mm × 400 mm × 400 mm) between 8:00 p.m. and 1:00 a.m. using a video tracking system (EthoVision® XT, version 15.0, Brain Science Idea Co., Ltd., Osaka, Japan). The mice were placed in the center of the arena and allowed to habituate for 30 min; locomotor activity was then recorded for 30 min [15].

Under intraperitoneal anesthesia, the left distal femur and bone mineral phantoms (QRM GmbH; Moehrendorf, Germany) were imaged using in vivo μCT (CosmoScan GX; Rigaku, Tokyo, Japan) with the following parameters: 90 kVp; 88 μA; voxel size, 10 × 10 × 10 μm^3; integration time, 35.714 ms; and scan time, 18 s. Using TRI/3D-BON software (Ratoc System Engineering, Tokyo, Japan), the change rate of trabecular volumetric BMD (Tb.vBMD) was calculated in a metaphyseal region of interest (ROI) with a height of 1.0 mm, commencing 0.5 mm proximal to the growth plate based on the value at week 0 [16]. At the end of the experiment, the mice were sacrificed at weeks 4 and 24, and the bilateral lungs and limb bones were removed for analysis.

2.3. Lung

Lung histomorphometry was performed as previously described [17]. Lungs at weeks 4 and 24 were inflated in 0.1 M phosphate-buffered saline (PBS) at a pressure of 25 cm H_2O and fixed with 4% paraformaldehyde (PFA) in 0.1 M PBS. After being embedded in paraffin, the lung tissue was cut into 5-μm-thick slices and stained with hematoxylin and eosin (H&E). H&*E*-stained sections were evaluated under a microscope using an image analysis and measurement system (WinROOF 2015; Mitani Corporation, Tokyo, Japan). In 20 randomly selected fields of the left lung parenchyma, the mean linear intercepts (Lm), a measure of mean alveolar diameter, were evaluated at 100× magnification, and the images were manually thresholded. Airway and vascular structures were excluded from the analysis.

2.4. Trabecular bone

The left femur was harvested at 4 and 24 weeks with mineral phantoms and was imaged using μCT with the following parameters: 90 kVp; 88 μA; voxel size, 10 × 10 × 10 μm^3; integration time, 533.33 ms; and scan time, 2 min. The analysis method and analysis area were the same as those used for the in vivo analysis, and the following parameters were calculated: trabecular bone volume (Tb.BV/TV: %), trabecular thickness (Tb.Th: mm), trabecular separation (Tb.Sp: mm), trabecular number (Tb.N: 1/mm), structural model index (SMI) and connectivity density (Conn.D: $1/mm^3$) [18,19].

The mice were given calcein (Fujifilm *Wako* Pure Chemical Corporation, Osaka, Japan) subcutaneously at 10 and 3 days before sacrifice. Right tibias were harvested at 4 and 24 weeks. Bone histomorphometry was performed on nondecalcified samples. Nondecalcified samples were examined using the same technique as in previous reports [16]. Each collected tibia was permeabilized in 70% ethanol for 3 days and embedded in methyl methacrylate (MMA) after Villanueva bone staining. Bone histomorphometry was measured using a semiautomatic analysis system (Histometry-RT, SYSTEM SUPPLY, Nagano, Japan). The analysis area was the secondary trabecular bone region, excluding the area within 250 μm of the growth plate and one cortical shell width of the intracortical surface. The following structural parameters were measured: bone volume/tissue volume (BV/TV: %), osteoid surface (OS/BS: %), osteoblast surface (Ob.S/BS: %), osteoblast number (Ob.N/BS: N/mm), osteoclast surface (Oc.S/BS: %), osteoclast number (Oc.N/BS: N/mm), mineralizing surface fraction (MS/BS; %), mineral apposition rate (MAR; μm/day) and surface referent bone formation rate (BFR/BS; mm^3/mm^2/year). The abbreviations for the histomorphometric parameters were derived from the recommendations of the Histomorphometry Nomenclature Committee of the American Society for Bone and Mineral Research [20,21].

2.5. Cortical bone

For the femoral bones removed at week 24, CT images were obtained using a microfocus X-ray CT (SMX-100CT, Shimadzu, Kyoto, Japan) under 70 kV and 70 μA radiation with a spatial resolution of 6 × 6 × 6 μm^3 to measure the cortical bone area (Ct.Ar: mm^2), cortical thickness (Ct.Th: μm), periosteal perimeter (Ps.Pm: mm) and endocortical perimeter (Ec.Pm: mm). To ensure sufficient spatial resolution for quantitative evaluation, the central part of the shaft was enlarged and photographed. After the CT images were binarized, the data were processed using TRI/3D-BON software (Ratoc System Engineering).

The degree of apatite *c*-axis orientation [22] as a bone quality parameter was analyzed using a μXRD system (R-AXIS BQ, Rigaku, Tokyo, Japan) equipped with a transmission-type optical system and an imaging plate (Fujifilm, Tokyo, Japan) placed behind the sample. The detailed conditions for μXRD were described in a previous paper [23,24] with minor modifications. The crystallographic *c*-axis of apatite aligns almost parallel to the collagen fiber direction because of the epitaxial crystallization of apatite on the collagen template; therefore, the degree of apatite *c*-axis orientation reflects that of the collagen fiber [25]. Mo-Kα radiation with a wavelength of 0.07107 nm was generated at a tube voltage of 50 kV and a tube current of 90 mA. The incident beam was focused on a beam spot 300 μm in diameter by a double-pinhole metal collimator and radiated in the anterior–posterior axis from the anterior surface at the center of the bone width. Diffraction data were collected for 600 s. The measurements were performed on the whole femur (Points 1–9). From the obtained diffraction intensity pattern, the degree of preferential orientation of the apatite *c*-axis along the bone axis was determined as the relative intensity ratio of the (002) to (310) diffraction peaks originating from apatite [26].

Three-point bending tests were conducted using a universal testing machine (Instron 5565, Instron, MA, USA) to evaluate flexural fracture behavior. The samples were loaded at a crosshead speed of 1 mm/min under moist conditions in HBSS and ambient temperature until failure. The maximum load (F_{max}, N), stiffness (S, N/mm), and energy-to-failure (U, N·mm) were analyzed from the load–displacement curve. Material properties such as the Young's modulus (E, GPa), maximum stress (σ_{max}, MPa) and toughness (μ, mJ/m^3) were calculated using the following equation.

$$E = S\frac{L^3}{48I_x} \tag{1}$$

$$\sigma_{max} = F_{max}\frac{L}{4Z_x} \tag{2}$$

$$\mu = U\frac{3}{L}\frac{y_{max}^2}{I_x} \tag{3}$$

where S is the stiffness, U is the energy-to-failure, F_{max} is the maximum load, L (mm) is the distance between the supports (8 mm in this study), I_x (mm^4) is the area moment of inertia, Z_x (mm^3) is the section modulus, and y_{max} (mm) is the maximum distance from the neutral axis to the outermost fiber of the cross-section. The values of structural parameters, including I_x, Z_x, and y_{max}, were analyzed using the CT data.

2.6. Bone marrow cells

The right femurs of the mice were harvested at week 24 and then trimmed on both ends of the femur, the intramedullary cavity was flushed with 0.1 M PBS, and the bone marrow cells were harvested. Total RNA preparation, single-stranded complementary DNA purification, and quantitative real-time polymerase chain reaction (qRT–PCR) analysis were performed as described previously [17]. The expression levels of each target gene were normalized to the expression level of the β-actin transcript.

Cap analysis gene expression sequencing (CAGE-seq) of bone marrow cells in both groups was performed as previously described [27]. Two samples (the saline group and the PPE group) were generated by pooling bone marrow cells from 4 mice per group. CAGE library preparation, sequencing, mapping and gene expression analysis were performed by DNAFORM (Kanagawa, Japan). The quality and quantity of total RNA were assessed using a bioanalyzer (Agilent, CA, USA) to ensure RNA integrity numbers (RINs) > 7.0 and A260/280 and A260/230 ratios >1.7. First-strand cDNAs were reverse transcribed from the RNAs, and second-strand cDNAs were subsequently synthesized and selected by the cap-trapping method. After the barcode tags were attached, CAGE libraries were constructed. Libraries were sequenced using 75-nt single-end reads on an Illumina NextSeq 500 sequencer. Reads were mapped to the mouse mm9 genome using BWA (version 0.7.12-r1039), and unmapped reads were then mapped using HISAT2 (version 2.0.5). The 5′ coordinates of the CAGE tags were clustered using the CAGEr R/Bioconductor package [28] with an irreproducible discovery rate (IDR) threshold of 0.1 [29] and a minimum count per million (CPM) of 0.1. Differential expression analysis was performed using DESeq2 [30]. Genes with |log2-fold change| > 1 and CPM > 10 were defined as genes meeting the expression-change criteria and classified as PPE-up or PPE-down for functional enrichment analysis using Metascape (https://metascape.org) [31]. Membership analysis was performed, and genes related to "mitochondria," "inflammation," "oxidative stress," and "hypoxia" were extracted to generate the respective gene lists. Because CAGE-seq was performed using one pooled sample per group, this analysis was considered exploratory and was used only for pathway screening, not for statistical inference of differential gene expression.

2.7. Statistical analysis

The primary outcome was the trabecular BV/TV of the distal femur assessed by μCT at 24 weeks after PPE or saline administration. Secondary outcomes include additional μCT indices, dynamic histomorphometric parameters of bone formation, bone material properties, mechanical properties from three-point bending, and physiological/behavioral measures. Because multiple secondary outcomes were assessed, secondary analyses were considered exploratory and interpreted accordingly.

The sample size was determined a priori based on the primary outcome (trabecular BV/TV by μCT at 24 weeks). Because variability estimates for 24-week BV/TV were not available at the planning stage, we used BV/TV data at 12 weeks from our prior study in this model as the basis for sample size planning (saline: 19.2 ± 2.4; PPE: 14.5 ± 3.6; values reported as standard deviation (SD), $n = 7$ per group). Using a pooled SD of approximately 3.06 and an expected between-group difference of 4.7, with a two-sided $\alpha = 0.05$ and 80% power for a two-group comparison, the minimum required sample size was estimated to be 7 mice per group. Accordingly, we planned to analyze 7 mice per group. A total of 15 mice per group were initially used for longitudinal assessments; the primary μCT endpoint (ex vivo BV/TV at week 24) was evaluated in the animals available at that time point ($n = 7$ per group), as indicated in the figure legends.

Differences in the mean Lm, bone morphometric parameters, and gene expression levels between the two groups were analyzed using the Mann–Whitney *U* test because of the nonnormal data distribution and limited sample sizes. Longitudinal changes in body weight, metabolic parameters, spontaneous locomotor activity, and Tb.vBMD assessed by in vivo μCT were analyzed using repeated-measures analysis of variance (ANOVA). The correlation between Lm and various parameters was analyzed using Spearman's correlation coefficient. A two-tailed *P* value <0.05 was considered to indicate statistical significance. All the statistical analyses were performed using GraphPad Prism (version 9; GraphPad Software, La Jolla, CA, USA).

3. Results

3.1. Open-field-assessed spontaneous locomotor activity after emphysema induction

There were no differences between the PPE and Saline groups at any time point in terms of body weight, feed intake, drinking volume, urine volume, fecal volume, or open-field-assessed spontaneous locomotor activity (Fig. 1B, C and Supplementary Fig. 1). Despite comparable feed intake and open-field-assessed spontaneous locomotor activity, compared with that in the Saline group, visceral fat mass in the PPE group was greater, whereas soleus muscle mass was lower (Supplementary Figs. 2 and 3). The values of Lm at weeks 4 and 24 in the PPE group were significantly greater than those in the Saline group (Fig. 1D).

3.2. Trabecular bone loss with impaired bone formation in mice with emphysema

The rate of change in the Tb.vBMD assessed by in vivo μCT was significantly lower in the PPE group than in the Saline group at weeks 8, 12, 16, 20, and 24, although the between-group difference appeared smaller at later time points (Fig. 2A).

Ex vivo μCT analysis revealed that the BV/TV and Tb.Th at week 24 were significantly lower in the PPE group than in the Saline group, although there were no significant differences in any bone microstructure parameters at week 4. Significant negative correlations were observed between Lm and BV/TV at week 24 (Fig. 2B and C).

With respect to bone histomorphometry of the proximal tibia at week 24, the BV/TV and osteoblast parameters were significantly lower in the PPE group. The dynamic parameters (MAR and BFR/BS) indicated impaired bone formation in the PPE group, and the osteoclast parameters did not significantly differ between the two groups. There were no significant differences in any parameters at week 4. Significant negative correlations were observed between Lm and BFR/BS at week 24 (Fig. 3A and B).

The mRNA expression levels of runt-related transcription factor 2 (Runx2), Sp7 transcription factor (Sp7/Osterix), collagen type I alpha 1 chain (Col1a1), and osteocalcin (OC), which are related to the differentiation and activity of osteoblasts, were significantly lower in the PPE group than in the Saline group (Fig. 3C).

3.3. Cortical bone with deterioration of bone quality in mice with emphysema

There were no differences in cortical BMD or morphological parameters in the central region of the femoral shaft between the two groups (Fig. 4A and B). However, regarding the orientation of the apatite *c*-axis, a significant decrease in the orientation was observed in the PPE group from positions 3–6 of the femoral shaft. Furthermore, a significant negative correlation was observed between the orientation of the *c*-axis of apatite at positions 4–5 and Lm (Fig. 5A).

Pentosidine in urine was significantly higher in the PPE group, and a significant positive correlation with Lm was observed (Fig. 5B). In mechanical testing, the values for energy-to-failure and toughness were significantly lower in the PPE group (Fig. 5C).

3.4. CAGE-seq analysis of bone marrow cells

Among 15,063 detected genes, 246 and 119 met the predefined criteria for lower and higher expression, respectively, in the PPE pooled sample. Membership analysis of each of these genes revealed a high percentage of genes related to "mitochondrial and oxidative stress" (PPE down: 47%, PPE up: 32%) (Fig. 6). The overall distribution of gene expression changes between the Saline and PPE groups is shown in Supplementary Fig. 4.

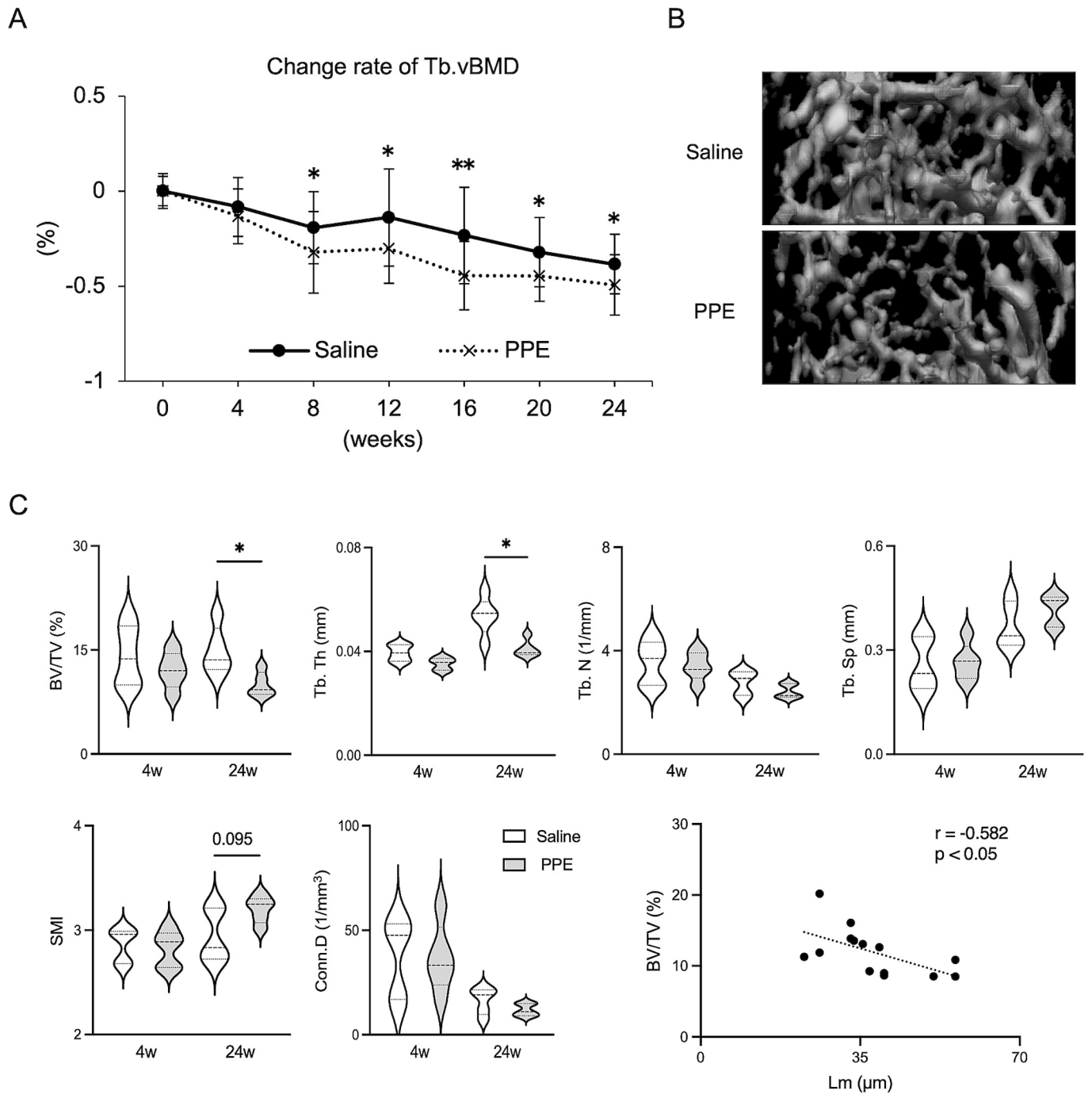

Fig. 2. Trabecular bone analysis assessed by μCT
(A) Sequential changes in trabecular volumetric bone mineral density (Tb.vBMD) in the distal femur as assessed by in vivo μCT. The data are presented as the mean ± SD ($n = 15$ mice per group). *P* values were determined by repeated-measures ANOVA. *$P < 0.05$. (B) Representative three-dimensional μCT images of trabecular bone within the region of interest (ROI) at the distal femur at week 24 (36 weeks of age). (C) Quantitative trabecular bone parameters within the ROI at weeks 4 and 24 ($n = 7$ mice per group). *P < 0.05. Violin plots indicate the probability density of the kernel, and the width of the shaded areas represents the proportion of data. The thick dashed line in the center indicates the median, the box represents the interquartile range, and whiskers indicate min–max values. The right panel shows the relationship between Lm and BV/TV within the ROI at week 24. The correlation coefficient r and *p*-value are shown in the upper right corner.

4. Discussion

In our study, elastase was administered intratracheally to induce pulmonary emphysema in mouse lungs, followed by a 6-month observation period. The results revealed that the bone microstructure deteriorated alongside impaired bone formation, leading to reduced material properties and bone strength. The absence of a between-group difference in open-field–assessed spontaneous locomotor activity is consistent with the possibility that emphysema-related factors contributed to the observed skeletal changes.

Patients with COPD have multiple fracture risk factors [9]. To investigate the impact of lung lesions on bone, it is necessary to exclude at least common fracture risk factors (age, smoking status, weight, malnutrition status, and habitual/daily physical activity level); however, this is difficult in clinical studies [10]. We previously conducted studies using this animal model but were unable to exclude the influence

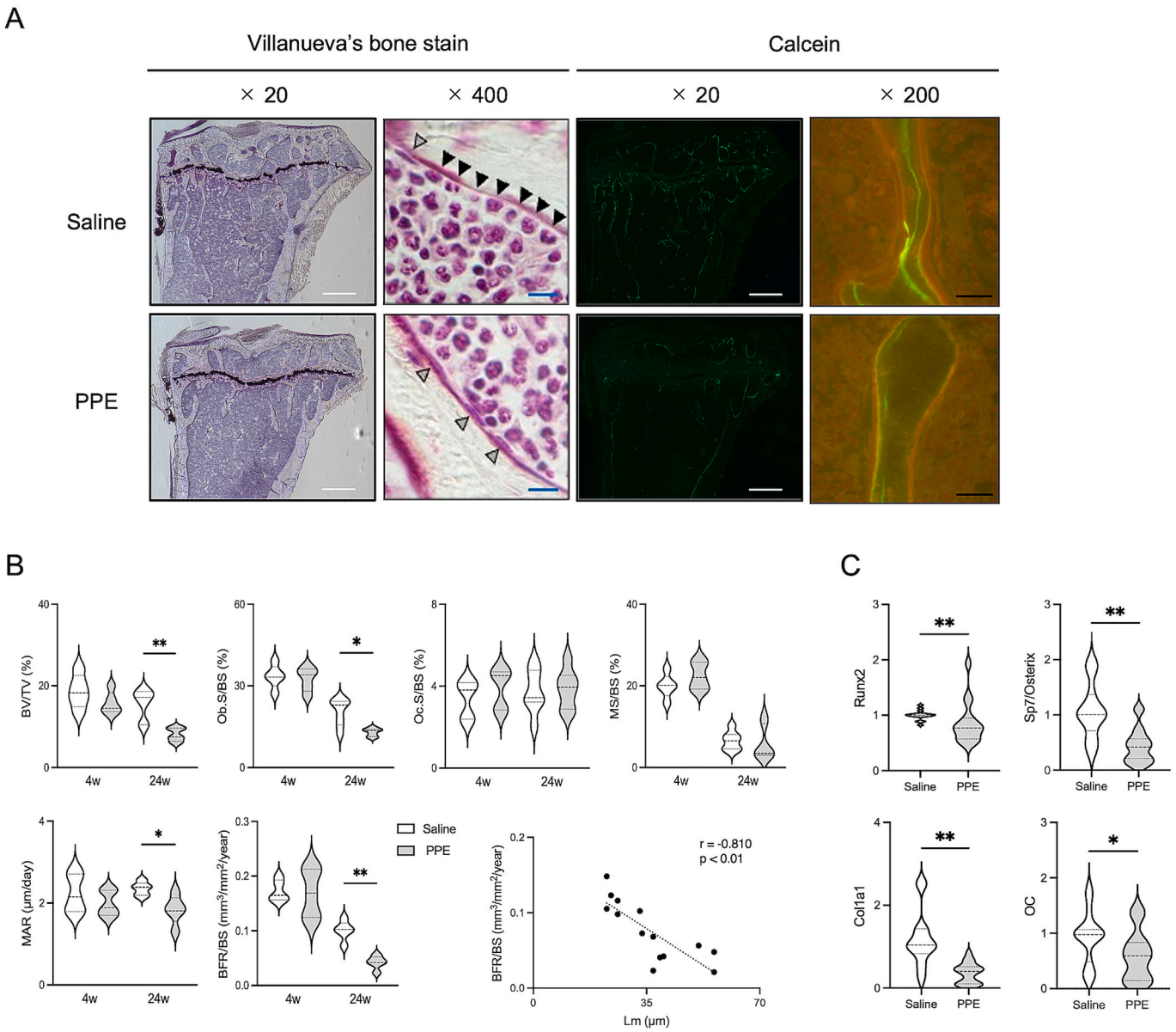

Fig. 3. Trabecular bone analysis by static and dynamic histomorphometry
(A) Representative light and fluorescence microscopy images of the proximal tibia at week 24. Scale bars: white, 500 μm; black, 50 μm; blue, 20 μm. (B) Quantitative trabecular histomorphometric parameters within the ROI at weeks 4 and 24 ($n = 5$–7 mice per group). *$P < 0.05$; **$P < 0.01$. The right panel shows the relationship between Lm and BFR/BS at week 24. The correlation coefficient r and p-value are shown in the upper right corner. (C) mRNA expression levels of Runx2, Sp7 (Osterix), Col1a1, and osteocalcin (OC) in bone marrow cells (n = 15 mice per group). *P < 0.05; **P < 0.01. Violin plots indicate the probability density of the kernel, and the width of the shaded areas represents the proportion of data. The thick dashed line in the center indicates the median, the box represents the interquartile range, and whiskers indicate min–max values. (For interpretation of the references to colour in this figure legend, the reader is referred to the web version of this article.)

of physical activity level [11]. Therefore, our study was the first to provide evidence that bone microstructure deterioration occurs in the presence of emphysema in a setting where spontaneous locomotor activity assessed by an open-field test did not differ between groups. Furthermore, material properties were also impaired. Although there was a slight difference in the Tb.vBMD of the distal femur at the final observation, bone strength was reduced, suggesting that emphysema strongly affects bone quality.

Material properties contribute to bone fragility through mechanisms independent of reduced bone density and deterioration of bone microstructure [32,33] and are related to oxidative stress [34–36]. In patients with COPD, serum hyperhomocysteinemia has been reported, and homocysteine generates reactive oxygen species, causing oxidative stress. In individuals under oxidative stress, reduced material properties lead to decreased bone strength [37–39]. Our study revealed reduced bone matrix orientation—one of the material property parameters—in the femurs of mice with emphysema, along with elevated urinary pentosidine levels and decreased bone strength. In this pooled, exploratory CAGE-seq analysis, approximately 40% of the genes meeting our expression-change criteria were related to oxidative stress and mitochondrial function. These findings suggest that oxidative stress may be involved in the bone phenotypes observed in this model. However, because the CAGE-seq analysis was performed using one pooled bone marrow sample per group, these findings should be interpreted as hypothesis-generating rather than confirmatory and currently remain within the scope of exploratory data. Although the CAGE-seq data in this

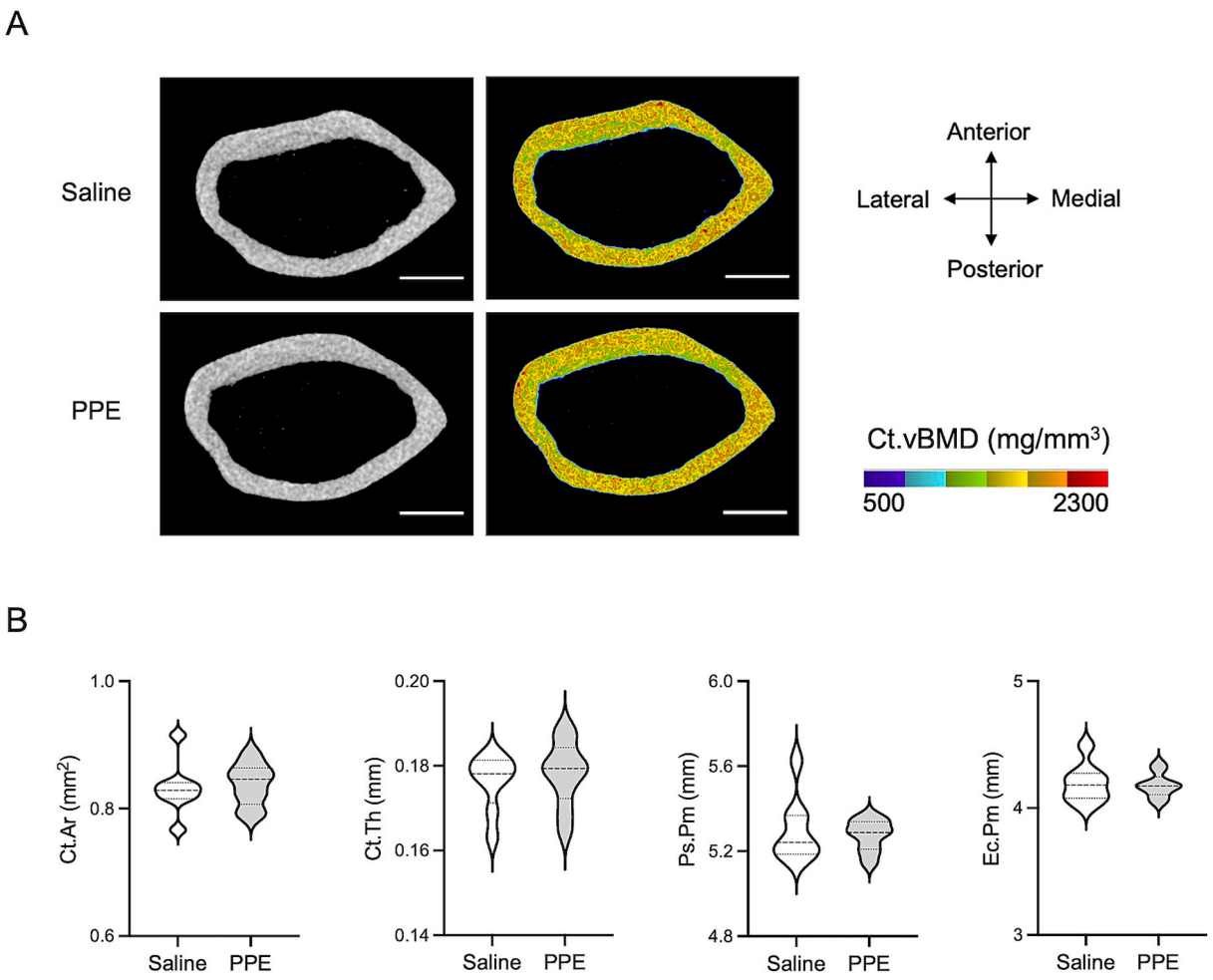

Fig. 4. Cortical bone analysis assessed by microfocus X-ray CT
(A) Representative three-dimensional images and bone mineral density mapping of cortical bone within the ROI at the femoral midshaft at week 24 (36 weeks of age). (B) Quantitative cortical bone parameters within the ROI of the femoral midshaft at week 24. Violin plots indicate the probability density of the kernel, and the width of the shaded areas represents the proportion of data. The thick dashed line in the center indicates the median, the box represents the interquartile range, and whiskers indicate min–max values (n = 8–10 mice per group).

study cannot be used to draw causal conclusions, antioxidant agents such as astaxanthin and sulforaphane are expected to improve bone quality, necessitating further investigation.

Although the shape parameters of the cortical bone in the femurs of the mice were identical, flexural fracture testing revealed a significant difference in energy absorbed (energy-to-failure) between the groups. Because energy-to-failure reflects the capacity for deformation (including post-yield deformation), a lower energy-to-failure suggests reduced post-yield deformation and increased brittleness. Oxidative stress reduces the orientation of apatite and decreases its mechanical properties [40,41]. Urinary pentosidine, a type of AGE and a substance generated within the body under the combined effects of oxidative stress, is increased in this model. Taken together, these findings are consistent with a possible contribution of oxidative stress to impaired bone material properties; however, the present study does not establish a causal relationship between oxidative stress, apatite disorientation, and bone brittleness.

There remains debate as to whether the musculoskeletal disorders observed in patients with COPD result from disuse or are changes attributable to the pathophysiology of emphysema. In this mouse model, bone quality deterioration and reduced bone formation were observed despite comparable open-field–assessed spontaneous locomotor activity and feed intake. Clinical studies have reported BMD-independent fracture risk in patients with COPD is not fully explained by BMD-defined osteoporosis [8]. Although the present model does not reproduce the full clinical spectrum of human COPD, this clinical observation is broadly consistent with the pattern observed in the present study. Furthermore, changes in visceral fat and muscle mass were observed in these model mice (Supplementary Figs. 1–3). It is well known that COPD patients have a high prevalence of metabolic syndrome [42]; therefore, further research using this mouse model may contribute to elucidating the mechanisms underlying lipid metabolism abnormalities in COPD patients.

The limitations of this study are as follows: Intratracheal administration of elastase was used to induce emphysema, but the same dose of elastase does not always induce the same severity of emphysema because the inhibitory effect of endogenous elastase activity varies among animal species and individuals. Therefore, although the major skeletal findings were consistently observed across the experimental cohorts, variations in the degree of lung injury may have contributed to the heterogeneity of the skeletal findings. Furthermore, although the experiment was conducted across multiple cohorts, the animals were randomly assigned to both groups, and no systematic differences related to the cohorts were observed during the data collection process. In addition, the elastase-induced pulmonary emphysema model is essentially a model of acute lung injury followed by emphysematous changes and thus is not a true COPD model. Nevertheless, this model is useful for investigating emphysema-associated skeletal changes. In addition,

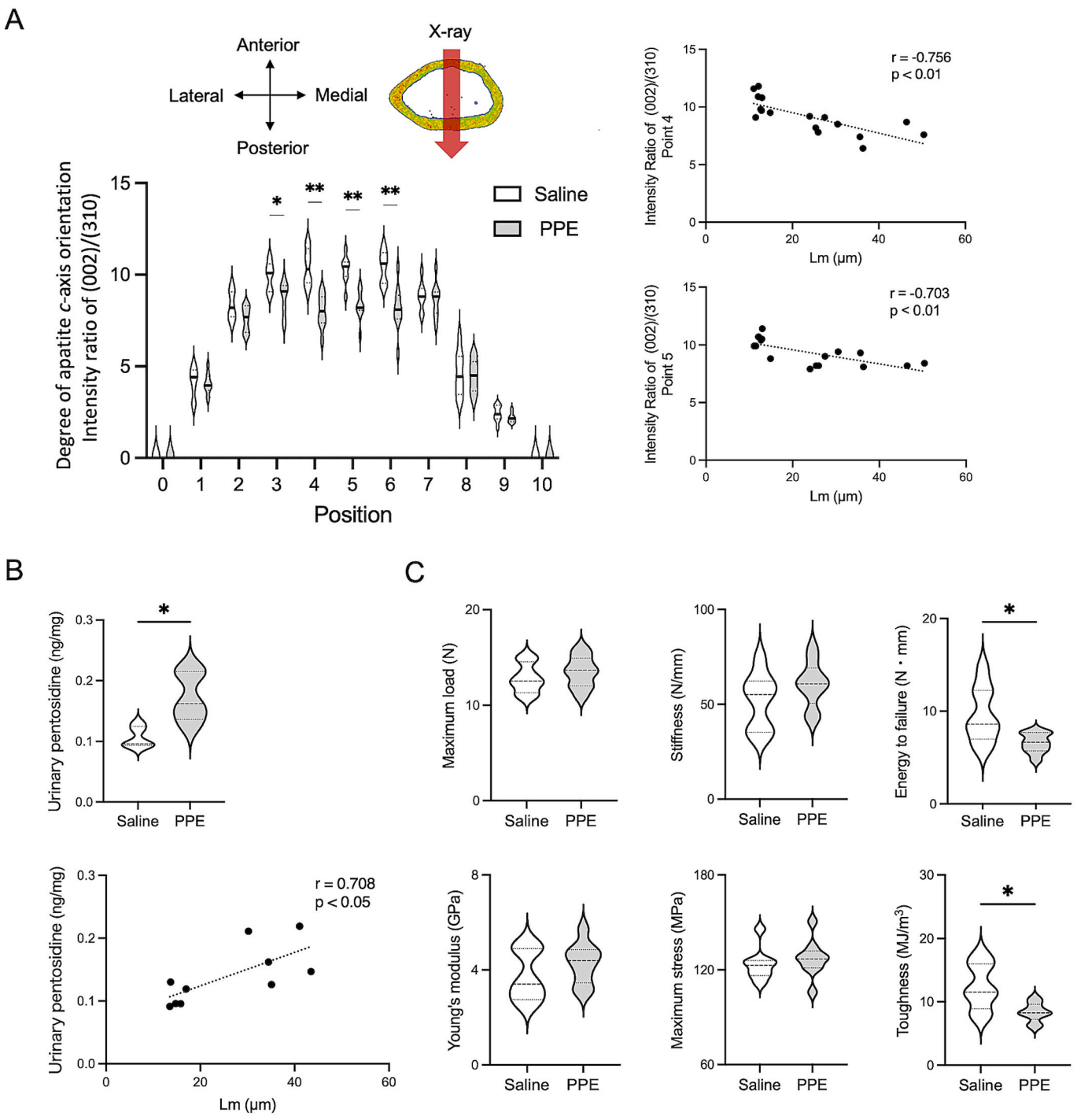

Fig. 5. Bone material properties and mechanical strength

(A) Degree of apatite *c*-axis orientation along the longitudinal axis of the femur at week 24 (n = 8–9 mice per group). *P < 0.05; **P < 0.01. The relationship between Lm and the orientation of the *c*-axis of apatite is also shown. The correlation coefficient r and p-value are shown in the upper right corner. (B) Urinary pentosidine concentrations at week 24 (n = 5 mice per group). *$P < 0.05$. The relationship between Lm and urinary pentosidine concentrations at week 24 is also shown. The correlation coefficient r and p-value are shown in the upper right corner. (C) Representative three-point bending test results and quantitative parameters of femoral bone strength, including maximum load, stiffness, energy-to-failure, Young's modulus, maximum stress, and toughness (n = 8–9 mice per group). *P < 0.05. Violin plots indicate the probability density of the kernel, and the width of the shaded areas represents the proportion of data. The thick dashed line in the center indicates the median, the box represents the IQR, and whiskers indicate min–max values.

locomotor activity was assessed using a 30-min open-field test, which captures behavior in a novel environment and may not fully reflect habitual home-cage activity over extended periods. Therefore, we cannot exclude subtle group differences in long-term daily physical activity, and interpretations related to physical activity should be limited to open-field–assessed locomotion. Future studies using continuous home-cage monitoring are warranted. Furthermore, as mentioned earlier, the bone marrow analysis performed in the present study was limited to exploratory pooled CAGE-seq analyses and did not evaluate changes in bone marrow cellular composition or lineage allocation. Therefore, we cannot determine whether alterations in specific marrow cell populations contributed to the impaired bone formation phenotype.

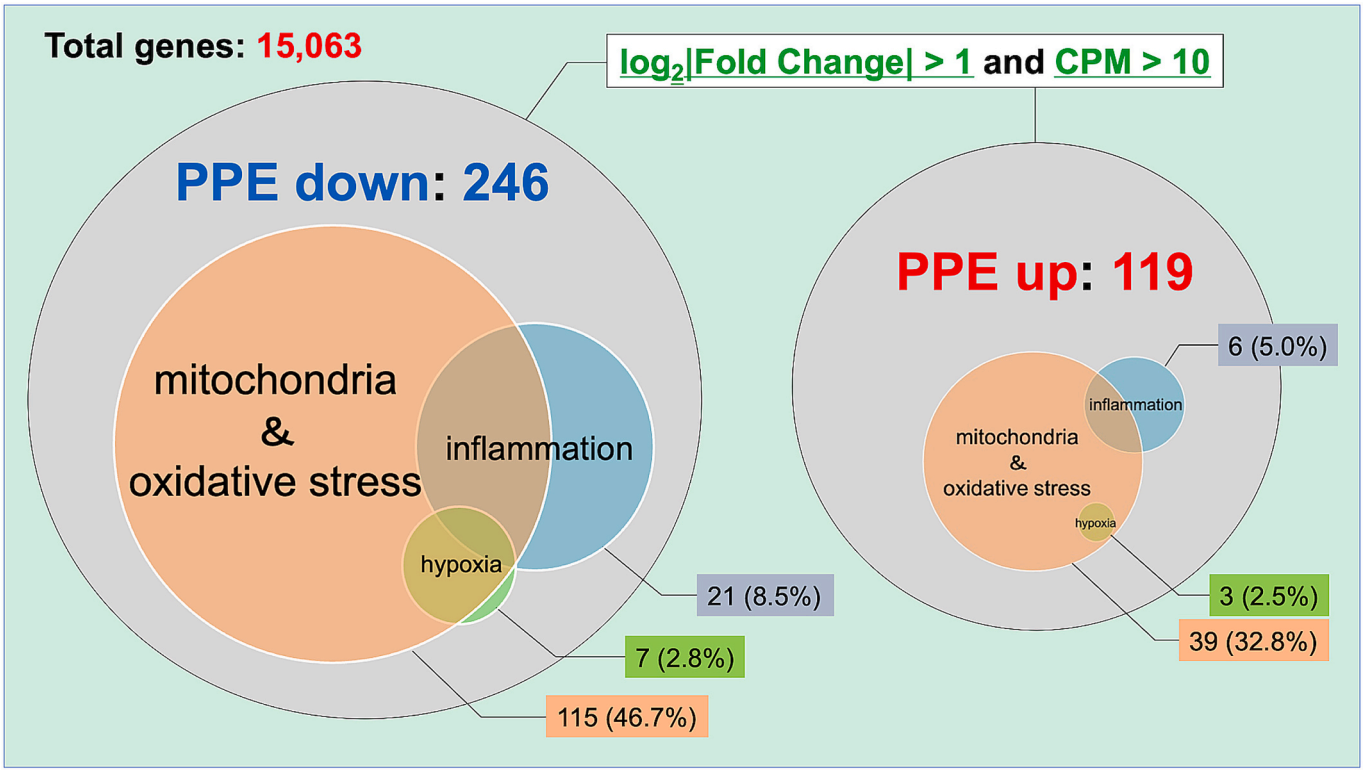

Fig. 6. CAGE-seq analysis of bone marrow cells
Among a total of 15,063 detected genes, 246 genes showed lower expression and 119 genes showed higher expression in the PPE pooled sample based on the predefined expression-change criteria. Gene ontology-based membership analysis revealed that a substantial proportion of the genes meeting the fold change and count per million thresholds were associated with mitochondrial and oxidative stress-related pathways (46.7% downregulated genes; 32.8% upregulated genes). These results are presented as exploratory, hypothesis-generating findings.

Future studies using flow cytometry, single-cell transcriptomics, or lineage-specific analyses will be necessary to clarify the cellular mechanisms underlying skeletal deterioration in emphysema. Finally, outcome assessments were not performed under blinded conditions. Although standardized acquisition and analysis protocols were used, observer bias cannot be completely excluded, particularly for image-based, histomorphometric, and mechanical outcome measures. The secondary outcomes (μCT data, histomorphometry, gene expression, material properties, and biomechanics) were evaluated using unadjusted multiple comparisons and are exploratory in nature. These limitations should be considered when interpreting the findings.

5. Conclusion

In the PPE-induced emphysema mouse model, open-field–assessed spontaneous locomotor activity was not reduced over 6 months, and physiological parameters such as body weight, feed intake, water intake, fecal output, and urine output were comparable between the groups. Despite preserved open-field–assessed spontaneous locomotor activity, emphysema was associated with deterioration of the trabecular microstructure and dynamic indices of bone formation, as well as impaired bone material properties (reduced apatite *c*-axis orientation and increased urinary pentosidine), resulting in decreased energy-to-failure and increased bone brittleness. These findings suggest that emphysema is associated with skeletal deterioration in a model with preserved open-field–assessed spontaneous locomotor activity; however, the contribution of differences in long-term habitual activity cannot be completely excluded.

CRediT authorship contribution statement

Takayuki Nabeshima: Writing – original draft, Investigation, Formal analysis, Data curation. **Manabu Tsukamoto:** Writing – review & editing, Supervision, Project administration, Funding acquisition, Conceptualization. **Ke-Yong Wang:** Supervision, Methodology. **Yosuke Mano:** Writing – original draft, Data curation. **Daisuke Arakawa:** Writing – original draft, Data curation. **Hitoshi Suzuki:** Writing – review & editing. **Eiichiro Nakamura:** Writing – review & editing. **Kazuhiro Yatera:** Writing – review & editing. **Ryosuke Ozasa:** Writing – original draft, Data curation. **Takayoshi Nakano:** Writing – review & editing, Supervision. **Akinori Sakai:** Writing – review & editing, Supervision.

Declaration of competing interest

M. Tsukamoto has received payments for lectures from Asahi Kasei Therapeutics Corporation and Amgen Inc. The other authors state that they have no conflicts of interest.

Acknowledgments

This work was supported in part by the Japan Society for the Promotion of Science Grants-in-Aid for Scientific Research (KAKENHI) (grant numbers JP 23K15702, 26K12184 [Manabu Tsukamoto] and 23H00235 [Takayoshi Nakano]) and the University of Occupational and Environmental Health Research Grant for Promotion of Occupational Health (2023–2024 [Manabu Tsukamoto] and 2025 [Yosuke Mano]). The authors gratefully acknowledge the American Society of Bone and Mineral Research 2023 Travel Award from the Japan Society of Bone and Mineral Research and the International Society of Bone

Morphometry 2024 Travel Award from the Japanese Society for Bone Morphometry. English language editing was provided by American Journal Experts. The funders played no role in the study design, data collection and analysis, decision to publish, or preparation of the manuscript.

Appendix A. Supplementary data

Supplementary data to this article can be found online at https://doi.org/10.1016/j.bone.2026.118035.

Data availability

Data will be made available on request.

References

[1] M. Decramer, W. Janssens, M. Miravitlles, Chronic obstructive pulmonary disease, Lancet 379 (2012) 1341–1351.
[2] P. Venkatesan, GOLD COPD report: 2025 update, Lancet Respir. Med. 13 (2025) e7–e8.
[3] A. Kjensli, P. Mowinckel, M.S. Ryg, J.A. Falch, Low bone mineral density is related to severity of chronic obstructive pulmonary disease, Bone 40 (2007) 493–497.
[4] F. Maltais, M. Decramer, R. Casaburi, et al., An official American Thoracic Society/European Respiratory Society statement: update on limb muscle dysfunction in chronic obstructive pulmonary disease, Am. J. Respir. Crit. Care Med. 189 (2014) e15–e62.
[5] A.I. Ritchie, J.R. Baker, T.M. Parekh, et al., Update in chronic obstructive pulmonary disease 2020, Am. J. Respir. Crit. Care Med. 204 (2021) 14–22.
[6] K. Ikezoe, T. Handa, K. Tanizawa, et al., Bone mineral density in patients with idiopathic pulmonary fibrosis, Respir. Med. 109 (2015) 1181–1187.
[7] R.Q. Graumam, M.M. Pinheiro, L.E. Nery, C.H.M. Castro, Increased rate of osteoporosis, low lean mass, and fragility fractures in COPD patients: association with disease severity, Osteoporos. Int. 29 (2018) 1457–1468.
[8] L. Graat-Verboom, B.E. van den Borne, F.W. Smeenk, et al., Osteoporosis in COPD outpatients based on bone mineral density and vertebral fractures, J. Bone Miner. Res. 26 (2011) 561–568.
[9] M. Tsukamoto, T. Nabeshima, K.Y. Wang, et al., The impact of chronic obstructive pulmonary disease on bone strength, J. Bone Miner. Metab. 42 (2024) 421–427.
[10] I. Kanazawa, M. Inaba, D. Inoue, et al., Executive summary of clinical practice guide on fracture risk in lifestyle diseases, J. Bone Miner. Metab. 38 (2020) 746–758.
[11] M. Tsukamoto, T. Mori, K.Y. Wang, et al., Systemic bone loss, impaired osteogenic activity and type I muscle fiber atrophy in mice with elastase-induced pulmonary emphysema, Bone 120 (2019) 114–124.
[12] M. Tsukamoto, T. Mori, E. Nakamura, et al., Chronic obstructive pulmonary disease severity in middle-aged and older men with osteoporosis associates with decreased bone formation, Osteoporos. Sarcopenia 6 (2020) 179–184.
[13] M. Tsukamoto, K. Menuki, T. Murai, et al., Elcatonin prevents bone loss caused by skeletal unloading by inhibiting preosteoclast fusion, Bone 85 (2016) 70–80.
[14] Y. Mano, M. Tsukamoto, K.Y. Wang, et al., Oxidative stress causes muscle structural alterations via p38 MAPK signaling in COPD mouse model, J. Bone Miner. Metab. 40 (2022) 927–939.
[15] O. Nikodijević, K.A. Jacobson, J.W. Daly, Locomotor activity in mice during chronic treatment with caffeine and withdrawal, Pharmacol. Biochem. Behav. 44 (1993) 199–216.
[16] D. Arakawa, M. Tsukamoto, K.Y. Wang, et al., Changes in bone metabolism dynamics in response to mechanical stress under pulmonary emphysema, J. Bone Miner. Metab. 44 (2026) 84–96.
[17] T. Nabeshima, M. Tsukamoto, K.Y. Wang, et al., Delayed cortical bone healing due to impaired nuclear Nrf2 translocation in COPD mice, Bone 173 (2023) 116804.
[18] M. Tsukamoto, K.Y. Wang, T. Tasaki, et al., Findings as a starting point to unravel the underlying mechanisms of in vivo interactions involving Wnt10a in bone, fat and muscle, Bone 120 (2019) 75–84.
[19] M.L. Bouxsein, S.K. Boyd, B.A. Christiansen, et al., Guidelines for assessment of bone microstructure in rodents using micro–computed tomography, J. Bone Miner. Res. 25 (2010) 1468–1486.
[20] A.M. Parfitt, M.K. Drezner, F.H. Glorieux, et al., Bone histomorphometry: standardization of nomenclature, symbols, and units, J. Bone Miner. Res. 2 (1987) 595–610.
[21] D.W. Dempster, J.E. Compston, M.K. Drezner, et al., Standardized nomenclature, symbols, and units for bone histomorphometry: 2012 update, J. Bone Miner. Res. 28 (2013) 2–17.
[22] T. Nakano, K. Kaibara, Y. Tabata, et al., Unique alignment and texture of biological apatite crystallites in calcified tissues, Bone 31 (2002) 479–487.
[23] R. Ozasa, M. Saito, T. Ishimoto, et al., Combination treatment with ibandronate and eldecalcitol prevents osteoporotic bone loss, Bone 157 (2022) 116309.
[24] R. Ozasa, A. Matsugaki, T. Ishimoto, et al., Bone fragility via degradation of bone quality in human rheumatoid arthritis, Bone 155 (2022) 116261.
[25] R. Ozasa, T. Ishimoto, S. Miyabe, et al., Osteoporosis changes collagen/apatite orientation and young's modulus, Calcif. Tissue Int. 104 (2019) 449–460.
[26] T. Nakano, K. Kaibara, T. Ishimoto, et al., Biological apatite crystallographic orientation as an index of bone regeneration, Bone 51 (2012) 741–747.
[27] H. Takahashi, S. Kato, M. Murata, P. Carninci, CAGE—cap analysis gene expression: a protocol for the detection of promoter and transcriptional networks, Methods Mol. Biol. 786 (2012) 181–200.
[28] V. Haberle, A.R.R. Forrest, Y. Hayashizaki, P. Carninci, B. Lenhard, CAGEr: precise TSS data retrieval and high-resolution promoterome mining for integrative analyses, Nucleic Acids Res. 43 (2015) e51.
[29] Q. Li, J.B. Brown, H. Huang, P.J. Bickel, Measuring reproducibility of high-throughput experiments, Ann. Appl. Stat. 5 (2011) 1752–1779.
[30] M.I. Love, W. Huber, S. Anders, Moderated estimation of fold change and dispersion for RNA-seq data with DESeq2, Genome Biol. 15 (2014) 550.
[31] Y. Zhou, B. Zhou, L. Pache, et al., Metascape provides a biologist-oriented resource for the analysis of systems-level datasets, Nat. Commun. 10 (2019) 1523.
[32] M. Saito, K. Marumo, Effects of collagen cross-linking on bone material properties, Calcif. Tissue Int. 97 (2015) 242–261.
[33] M. Saito, K. Marumo, Collagen cross-links as a determinant of bone quality, Osteoporos. Int. 21 (2010) 195–214.
[34] M. Saito, K. Fujii, Y. Mori, K. Marumo, Role of collagen cross-links in diabetic rats, Osteoporos. Int. 17 (2006) 1514–1523.
[35] M. Saito, K. Marumo, S. Soshi, et al., Raloxifene ameliorates collagen cross-links, Osteoporos. Int. 21 (2010) 655–666.
[36] H. Nojiri, Y. Saita, D. Morikawa, et al., Cytoplasmic superoxide causes bone fragility, J. Bone Miner. Res. 26 (2011) 2682–2694.
[37] F. Folchini, N.L. Nonato, E. Feofiloff, et al., Oxidative stress markers in COPD, Chron. Respir. Dis. 8 (2011) 101–108.
[38] F.L. Fimognari, L. Loffredo, S. Di Simone, et al., Hyperhomocysteinemia in COPD, Nutr. Metab. Cardiovasc. Dis. 19 (2009) 654–659.
[39] S. Kai, A. Nomura, Y. Morishima, et al., Smoking-related hyperhomocysteinemia in COPD, Arch. Gerontol. Geriatr. 42 (2006) 117–124.
[40] T. Wakamatsu, Y. Iwasaki, S. Yamamoto, et al., Angiotensin II receptor blockade improves bone material properties, J. Bone Miner. Res. 36 (2021) 67–79.
[41] Y. Shinno, T. Ishimoto, M. Saito, et al., Advanced glycation end-products diminish dentin strength, Sci. Rep. 6 (2016) 19849.
[42] H. Alrabbaie, M. Al-Wardat, M. Etoom, M. Beauchamp, R. Goldstein, D. Brooks, The prevalence of metabolic syndrome in chronic obstructive pulmonary disease: a systematic review and meta-analysis, Chron. Respir. Dis. 22 (2025) 14799731251346194.